Research Article

Gunawan Dwi Haryadi, Rando Tungga Dewa*, I. M. W. Ekaputra, and Agus Suprihanto

Investigation of post-weld heat treatment (T6) and welding orientation on the strength of TIG-welded AL6061

https://doi.org/10.1515/eng-2020-0084
Received Jan 03, 2020; accepted Jun 04, 2020

Abstract: This paper investigates the influence of T6 post-weld heat treatment (PWHT), and welding orientation on the strength and microstructure of tungsten inert gas (TIG) welded AL6061 aluminum alloy. The TIG process was used to weld the AL6061 at the transversal and longitudinal orientations with reference to the rolling direction. The T6-PWHT is a two-phase heat treatment process, and was applied to AL6061 in order to increase its strength. This T6 was carried out under three different artificial aging; 8, 18, and 24 hours. The influence of PWHT and welding orientation on the strength of AL6061-T6 were investigated through a series of tensile and microhardness tests. In addition, the microstructure observations were performed using the optical and scanning electron microscopes. It was established that the strength and microstructural characteristics of AL6061 are significantly dependent on the T6 artificial aging. Accordingly, the improvements in the strength and ductility were mainly contributed by the grain growth and subsequent precipitate strengthening. Moreover, the welding orientation only affects their fracture surfaces and locations after tensile testing.

Keywords: Aluminum alloy, Post weld heat treatment (PWHT), Mechanical strength, Tungsten inert gas (TIG) welding, Welding orientation.

1 Introduction

By having excellent mechanical properties, high corrosion and fatigue resistance, lightweight ratios, low cost, and good weldability, the aluminum-magnesium-silicon (Al-Mg-Si) denotes as 6xxx series alloy is widely used for fabrication of critical structural components in the aircraft and aerospace industries. The application requires high strength and ductility of the material to restrain such mechanical loadings in operation. The AL6061 is a precipitation hardening Al alloy with a high content of Mg and Si elements. The Mg contents will significantly improve its strength, and the silicon will enhance the castability and high-temperature crack resistance of AL6061.

For fabrication of large structures, a solid state joining can be used for welding of AL6061 [1, 2]. In the welding process, the microstructure heterogeneity will occur between the weld metal (WM) and base metal (BM) afterwards, which will cause the differences in mechanical properties. Therefore, a suitable welding method must be employed for producing and designing a good welded product. The tungsten inert gas (TIG) welding is the most extensive gas shielded arc-welding process that can be applied in joining Al alloys due to their flexibility and relatively low-cost production. TIG welding can produce a high-quality and stable process, which has less spatter characteristics and better weld bead appearance. Currently, the TIG welding has attracted the scientific interest because of the difficulties for ensuring the integrity and reliability at the joints of Al alloys. Previous works use TIG welding for thin Aluminum sheet, and thus, has more advantageous other than conventional welding methods [3, 4]. However, further investigation is remained to improve the mechanical strength and determine the welding parameters of the TIG-welded AL6061.

Numerous reports have been published in the past years in the investigation of post-weld heat treatments (PWHT) on the AL 6061. Eltai *et al*. investigated the influence of PWHT on the corrosion behaviour of the TIG-welded AL6061-T6 [2]. According to his findings, the TIG-

***Corresponding Author: Rando Tungga Dewa:** Indonesia Defense University, IPSC Area, Sentul, Bogor, West Java 16810, Indonesia; Email: rando.td@gmail.com
Gunawan Dwi Haryadi, Agus Suprihanto: Diponegoro University, Jl. Prof. Sudharto, SH., Tembalang-Semarang 50275, Indonesia
I. M. W. Ekaputra: Sanata Dharma University, Paingan, Maguwoharjo, Depok, Sleman-Yogyakarta, 55282, Indonesia

welded led to a reduction of microhardness in the area of the WM, and the most significant decline was found in the heat-affected zone (HAZ). Literature studies show that the PWHT had been successfully used to improve the properties of WM that give it particular characteristics [1, 2]. The PWHT is well-known to enhance the performance of the WM since the increase in temperature will form generous precipitations to various degrees. Based on many investigations, they approved that the T6 artificial aging process is well-applied to AL6061. It is also noticed that the T6 process on Al alloys can dissolve the β phase (Mg_2Si), homogenize the solid solution, and spheroidize the eutectic Si. Although, there are several works of literature reported the influence of the PWHT on the microstructure of AL6061, yet, there are still excessively data set needed regarding the implication of PWHT on the mechanical performance of the AL6061.

In the complex geometry, the welding process is not always inline within the rolling direction on the metal plate due to the impediment in application. Since the WM will undoubtedly affect the deformed zone and strain localization during service loadings, one of the other set parameters to be understood is the appropriate characteristic of welding orientation. Therefore, in this paper, the investigation is focused on the combination of PWHT under three different artificial aging at 8, 18, and 24 hours and the welding orientation, which was welded at the transversal and longitudinal axis concerning the rolling direction, thus, to improve the strength and microstructure of the TIG-welded AL6061.

2 Research Methods

2.1 Specimen Preparations

The AL6061 aluminum alloy BM plates with the dimensions of 400 × 300 × 2.5 mm were joined by TIG welding process. Prior to the welding process, the Al alloy plates were polished and cleaned to eliminate the impurities. This TIG process used the heat generated by an electric arc between the metals to be joined and a non-consumable tungsten electrode, located in the welding torch. The arc area was shrouded in an inert gas shield to protect the weld pool and the tungsten electrode. The filler metal as a rod was applied manually into the weld pool. The ER4043 filler wire was chosen for the process due to its good fluidity and most importantly, resistance to crack (excellence choice for PWHT specimens). The filler material ER4043 was utilised to fill the weld groove and bonding the two surfaces. The non-consumable tungsten electrode used in this investigation has a dimension of 1.6 mm in diameter to produce the WM. Figure 1 shows the energy-dispersive x-ray spectroscopy (EDS) analysis of AL6061 for BM and WM for chemical characterisation. Based on the results, Silicon composition is evident in the WM part due to the utilisation of ER4043 Al-Si filler wire. The complete chemical compositions of AL6061 Aluminum alloy BM and ER4043 filler wire material are listed in Table 1.

The miller welding machine was used with manual process by the welder. The details of welding parameters used in this investigation are listed in Table 2. The AL6061 BM plates were TIG welded and hot-rolled by following several testing conditions, such as welding longitudinal rolling longitudinal (WLRL), welding longitudinal rolling transversal (WLRT), welding transversal rolling longitudinal (WTRL), and welding transversal rolling transversal (WTRT). After welding, the as-welded plate was subjected to the PWHT (T6) process. The PWHT (T6) is a two-phase process, which was applied to AL6061 in order to increase the strength. The detail steps and procedures of the T6 artificial aging is shown in Figure 2. The T6 two-phase process

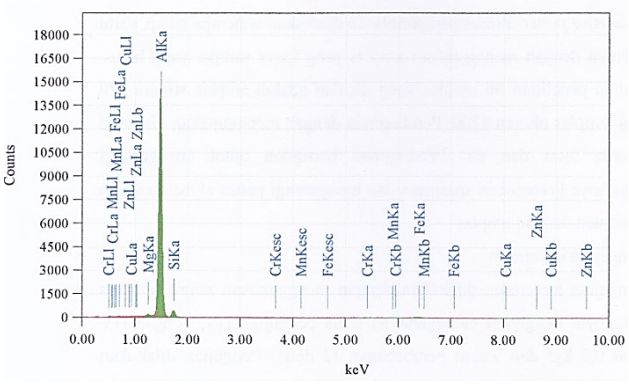

(a)

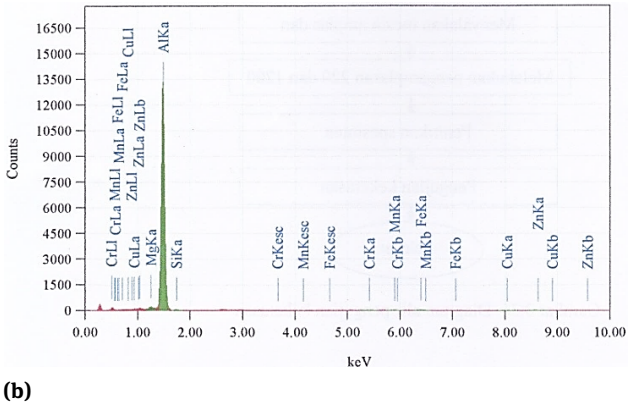

(b)

Figure 1: The energy-dispersive x-ray spectroscopy (EDS) results of AL6061 (a) BM; and (b) WM.

Table 1: The chemical Composition of AL6061 and Wire Filler ER4043 (wt%).

References	Al	Si	Fe	Cu	Mn	Mg	Cr	Zn	Ti	Etc.
AL 6061 (BM)	96.07	0.64	0.9	0.38	0.35	1.03	0.33	0.30	-	-
AL 6061 (WM)	89.86	7.22	1.03	0.38	0.29	0.82	0.10	0.30	-	-
ER 4043	Bal	4.8	0.2	0.02	<0.01	0.01	-	0.02	0.01	<0.15
ASM Spec.		0.4-0.8	0.7	0.15-0.40	0.15	0.8-1.2	0.04-0.35	0.25		

Table 2: The welding parameters used in this investigation.

Parameters	Value
Welding equipment	Miller
Tungsten electrode diameter	1.6 mm
Filler wire diameter	2.4 mm
Heat input	2.5kJ/mm
Peak current	70 Amps
Base current	60 Amps
Peak voltage	14.3 Volts
Base voltage	13.8 Volts
Welding speed	4.19 mm/sec
Welding grade	99.9995%
Pulse frequency	6 Hz
Pulse on time	50%
Shielding gas	Argon
Gas flow rate	15 L/min

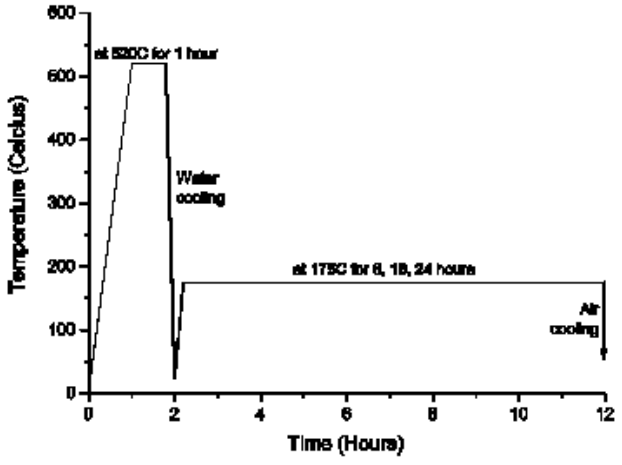

Figure 2: The PWHT (T6) process diagram.

was initiated by the rapid increase of temperature from room temperature (RT) until 520°C and was held for 1 h. After 1 h, the as-welded plate was quenched in water until 175°C and subsequently applying the T6 artificial aging for 8, 18, and 24 hours, respectively. This process is expected to cause extensive grain growth across the WM, and consequently improving the strength.

2.2 Test Methods

The Vickers microhardness tests were conducted across the plate with 0.3 kgf of indentation load and 12 secs of dwell time, as recommended in ASTM E384-16 [5]. The indentations were set at the centre position from the WM area to the BM area every 1 mm, as schematically shown in Figure 3. The tensile test specimen used in this investigation was rectangular in shape, and the dimension can be seen in Figure 4. The WM specimens were specifically machined to the required dimensions from the weld pad, as shown in Figure 4(b). Series of tensile tests were conducted in RT laboratory environment with a tension rate at 1 mm/min. These test specifications were adjusted with the standard of ASTM B557 [6].

The samples for microstructure examinations were perpendicularly extracted from the fractured specimens after tensile testing. The samples were polished and etched with Keller's reagent containing 2.5 ml of HNO_3, 1.5 ml of HCl, 1 ml of HF, and 95 ml of H_2O for 10-20 secs to reveal their microstructure. Microstructural characterization was performed via optical microscope (OM) and scanning electron microscope (SEM) coupled with energy-dispersive x-ray spectroscopy (EDS) equipment. The grain measurement was carried out using the linear intercept method from the microstructure image, as recommended in the ASTM E112 [7].

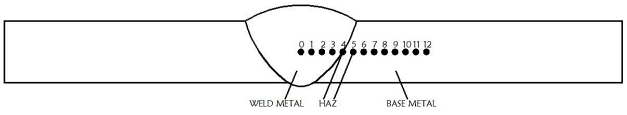

Figure 3: Welding profiles (BM, HAZ, and WM) across the plate and schematic illustration of microhardness test path.

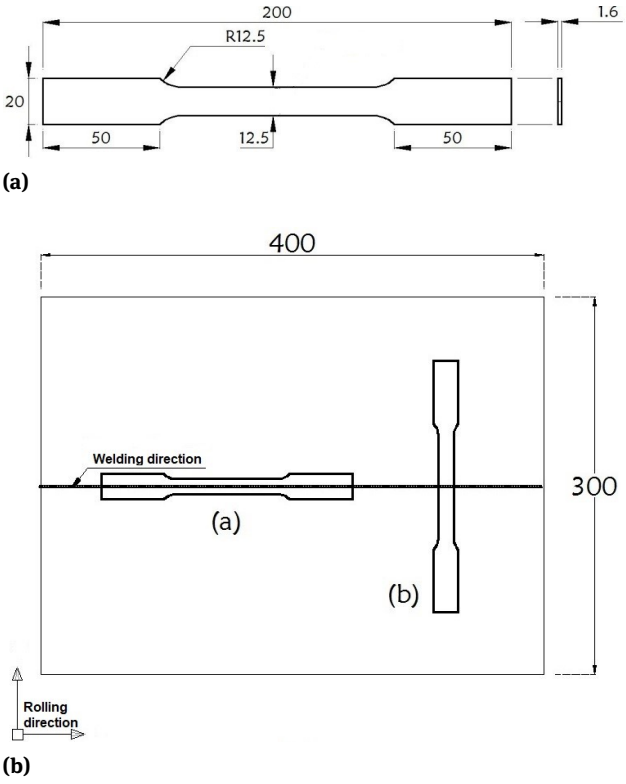

Figure 4: (a) The tensile test specimen geometry; and (b) Configuration for longitudinal and transversal direction of the welding and rolling orientation (all units are in millimetres).

3 Results

3.1 Microstructure

Figures 5 and 6 show typical OM images of the AL6061-T6 after 24 hours of aging compared with the as-welded AL6061. From the figures, the dual phases can be observed as the bright colour for the solid Al solution (Al-matrix), and a darker colour for low melting phase (Mg-Si) of AL6061-T6 specimens. Similar finding revealed that these Mg and Si are bound each other into Mg_2Si precipitate at particular temperature environment but a quite low solubility at RT, generating a precipitate strengthening property [8]. It is clearly seen that larger size and amount of precipitates are desirable due to the PWHT in comparison with the as-welded AL6061.

After TIG welding, the heterogeneity between microstructure occurred within the WM and BM region due to the heat. The WM is surrounded by the HAZ, the area that had its microstructure and properties altered by the welding. These each microstructure have different properties depend on the BM and filler metal used when subjected to heat. The uniform equiaxed dendritic grain type can be seen in the WM. The microstructure of AL6061-T6 consists of α-Al dendrites and eutectic Si particles along the dendritic grain boundaries (GBs) and the grain configuration is more uniformly dispersed and reduced in size after heat-treatment. This finding is coincided as in Ref. [9]. While the precipitate strengthening mechanism can be illustrated as the interaction of the recurrent dislocation, which is hindered by precipitate particles (Mg_2Si) [10]. If the particle is massive and hard, the driving force results mainly in a significant enhancement of the strength. Furthermore, if the driving force is attained, thus the precipitate will be sheared, or the moving dislocation will pass through (looping) for the hard enough particle.

The grain growth measurement was conducted using the linear intercept method, as schematically illustrated in Figure 7. Figure 8 shows the average grain size results under different set-up parameter conditions for WM and HAZ. Based on the results, the average grain size tends to decrease with an increase in the T6 artificial aging. Variation in T6 aging process is affecting the grain growth after recrystallization, resulting in smaller grain size in the WM and HAZ microstructure.

3.2 Microhardness Analysis

The exact extension of the HAZ and WM region are not easily measurable. Thus, each indentation of the microhardness is drawn based on the average points. Previous report said that the microhardness can be affected by dissolving precipitates in grains, and GBs called precipitation hardening due to the PWHT [11]. The variation of microhardness on the WM, HAZ, and BM (taking origin at the centre of the WM) for longitudinal and transversal welding orientation specimens are shown in Figure 9. For as-welded specimen, the profile exhibits that the WM has the highest microhardness compared to the HAZ and BM. The highest microhardness of the WM is two times more than the BM. However, after PWHT, the microhardness significantly increased compared to the as-welded specimen and nearly uniform in the WM, HAZ, and BM. It is also obtained that the highest microhardness is observed at 24 hours aging for both transversal and longitudinal welding, which are 114.4 HV and 124 HV, respectively.

3.3 Mechanical Properties of the TIG-welded AL6061

Figure 10 shows the tensile test results of the AL6061-T6. It is shown that the yield strength (YS) and ultimate ten-

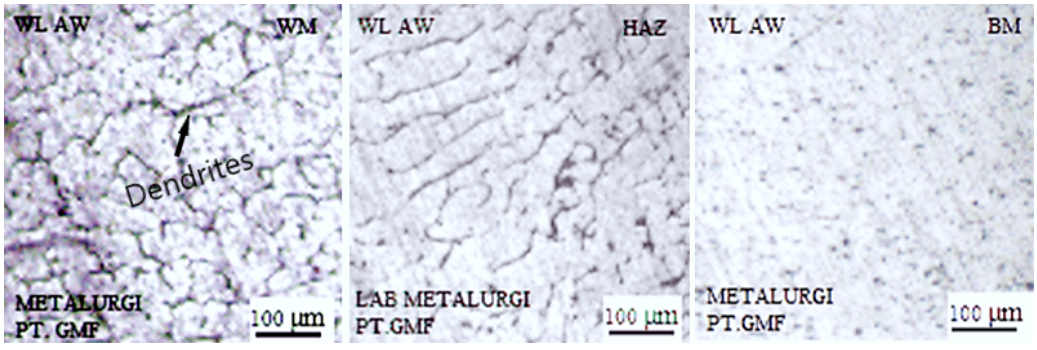

(a)

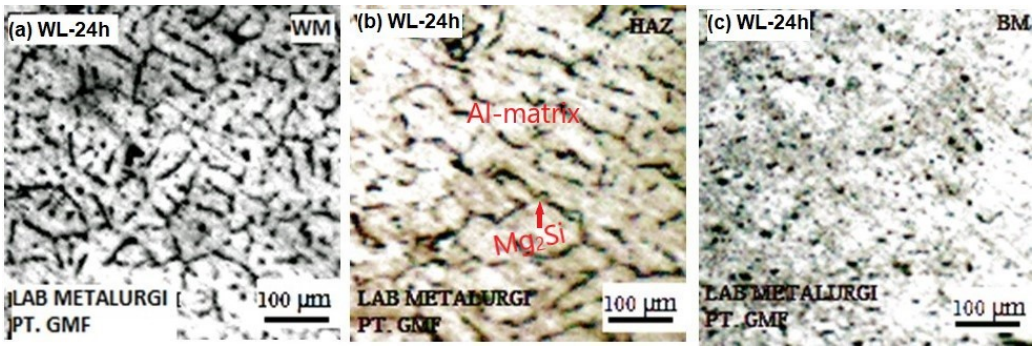

(b)

Figure 5: OM images as a comparison of; (a) As-welded AL6061, and (b) AL6061-T6 aged for 24 hours on longitudinal welding orientation for WM, HAZ, and BM (left to right).

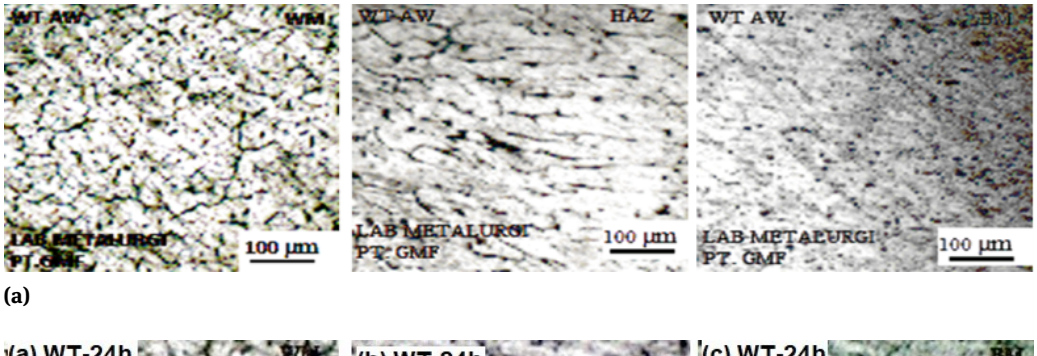

(a)

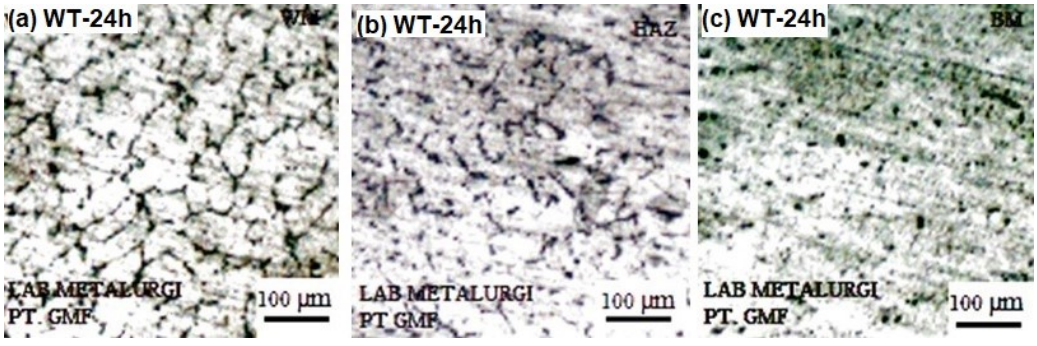

(b)

Figure 6: OM images as a comparison of; (a) As-welded AL6061, and (b) AL6061-T6 aged for 24 hours on transversal welding orientation for WM, HAZ, and BM (left to right).

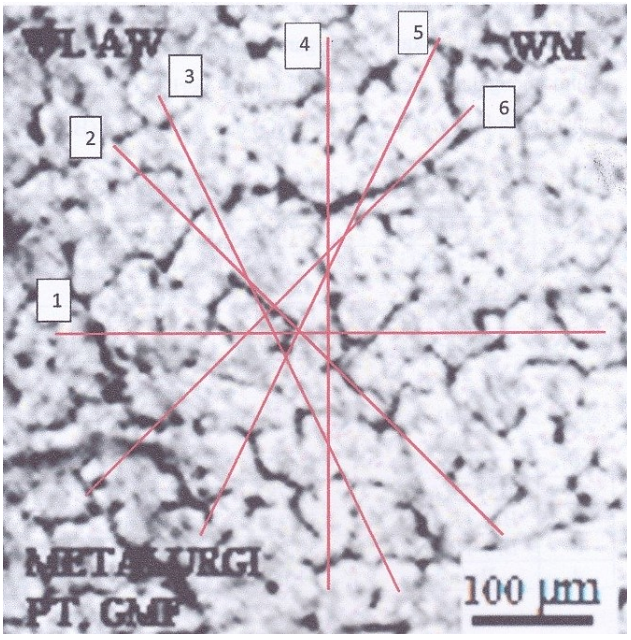

Figure 7: Conception of the linear intercept method to measure the grain size for the as-welded specimen [5].

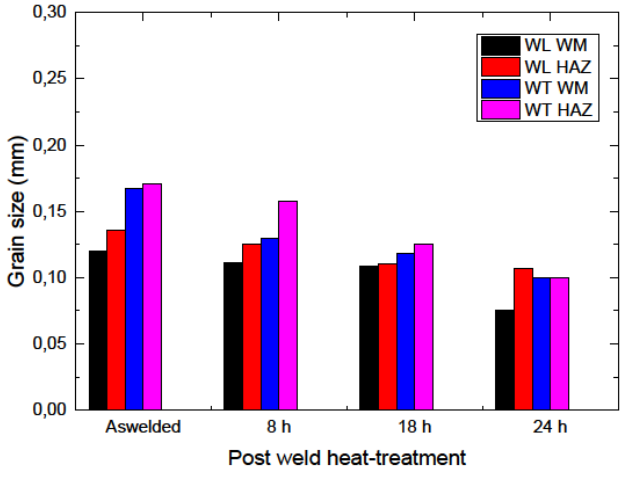

Figure 8: Average grain size measurement for as-welded AL6061 and AL6061-T6 especially for WM and HAZ.

sile strength (UTS) are increased along with an increase in T6 artificial aging. The T6 at 24 hours is found to have the most superior YS and UTS. However, after T6 (>8 hours) the strength of transversal welding is lower compared to the longitudinal welding. The tensile test results are in a good agreement with the results from the microhardness test and grain size measurement. It has been reported that the grain growth and strengthening mechanism after T6 process enhanced the strength of the TIG-welded AL6061 since the T6 took over the process [10–12]. The dissolution and growth of precipitates were developed in a range of

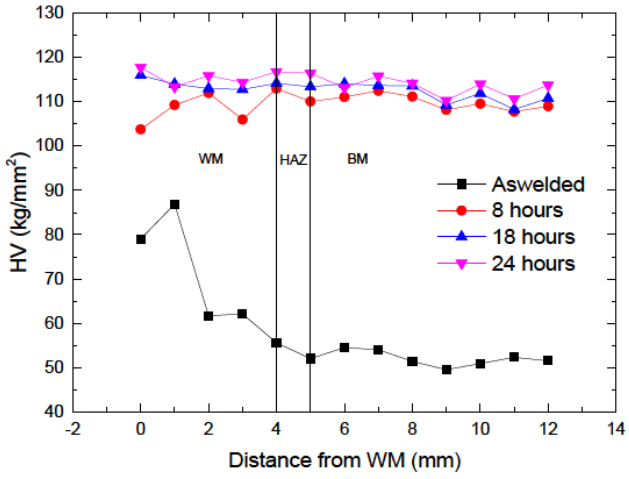

(a)

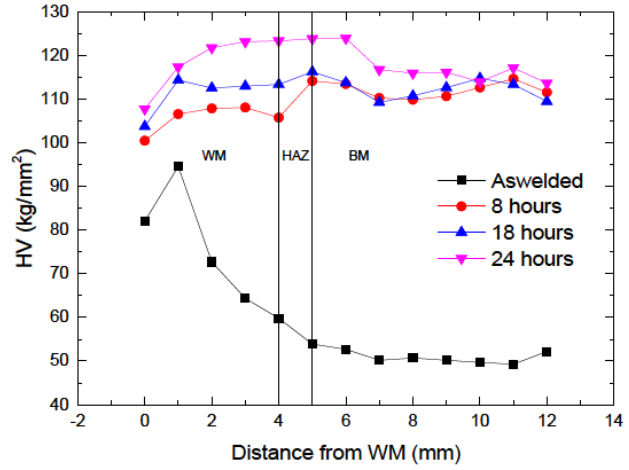

(b)

Figure 9: Vickers micro-hardness profiles distribution across the WM specimen; (a) Longitudinal, and (b) Transversal welding.

T6 artificial aging, meaning more precipitates were developed along with a long period of T6 aging, as it is seen in the Figures 5-6. With an increase in precipitates number, and the strength is expected to increase. It has been also reported that the skinny needles and high density of β''-type precipitates were observed in the interior of AL6061-T6 microstructure [12–16]. Those precipitates served as obstacles to block the movement of dislocations during deformation. Dislocations are recognized to be the site for heterogeneous nucleation and paths for increasing the atomic movement during growth. These changes are again associated with the variation in the temperature experienced in the different T6 artificial aging, which in turn affects the dissolution or coarsening of precipitates. In another case, the elongation is decreased along with an increase in T6 artificial aging. However, the longitudinal WM specimens have higher ductility than the transversal WM specimens.

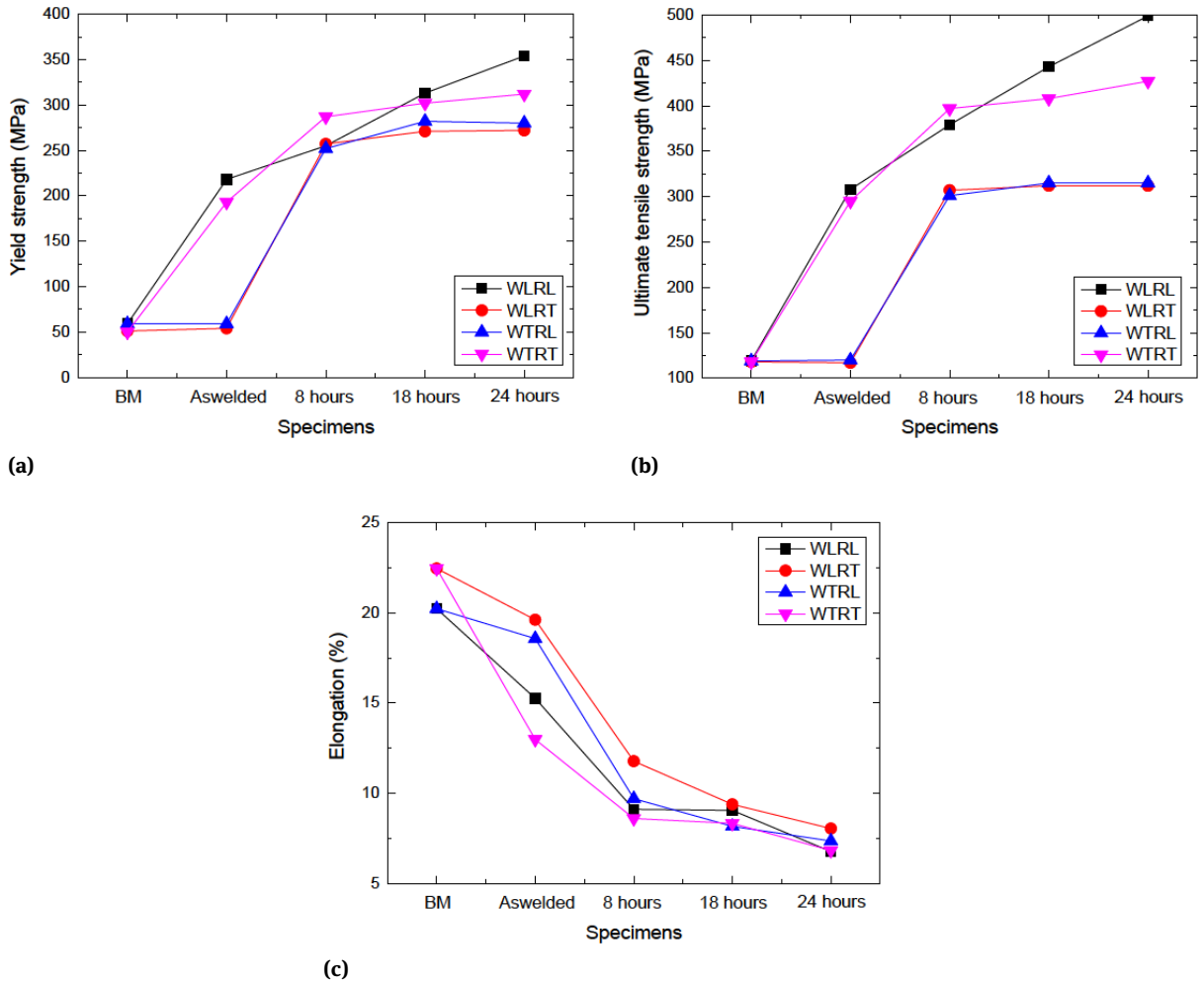

Figure 10: The tensile test results of the AL6061-T6 at RT; (a) Yield strength, (b) Ultimate tensile strength, and (c) Elongation.

Figure 11: Typical fractured specimens from tensile tests, showing the fracture location of the AL6061 BM and WM.

It is noted that, if the welding and rolling direction is in the same line, the mechanical properties is the most superior compared to that with other set-up parameters.

3.4 Fracture Behaviour

Figure 11 shows the representative fractured samples of BM and TIG AL6061. For BM, the fracture location is located in the middle of the specimen with a cup-and-cone fracture shape, indicating a ductile fracture. For the WM longitudinal specimens, fracture location has encompassed the WM, HAZ, and BM regions with flat-type fracture, and somewhat sheared due to the high strength of WM. In the case of the transversal WM samples, fracture location is also located in the BM with a cup-and-cone fracture shape. In this case, the strength was required to restrain the deformation during tension. Meanwhile, the WM has higher strength rather than the BM, and in other words, the strain was localized in the lower strength zone, namely BM until fracture. Figure 12 shows typical SEM images of as-welded AL6061 and AL6061-T6 for 24 hours of WLRL specimens. Based on this observation, the morphologies

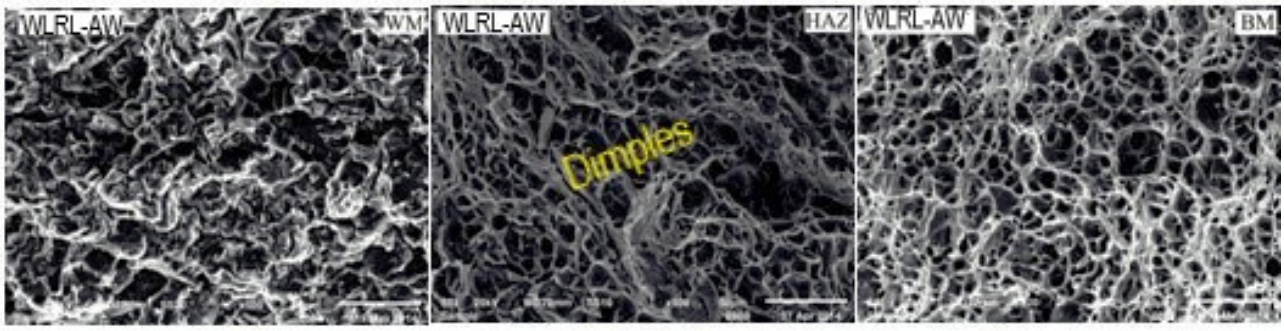

(a)

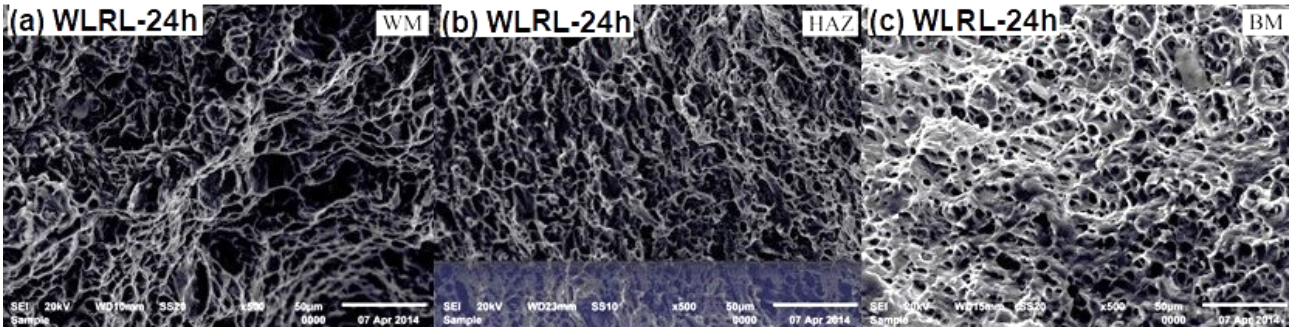

(b)

Figure 12: Typical SEM fractographs of; (a) As-welded AL6061, and (b) AL6061-T6 aged for 24 hours on WLRL specimen, indicating WM, HAZ, and BM (left to right).

of fractures include a great number of fine dimples which are distributed uniformly on the fracture surface. A ductile fracture is seen in as-welded sample accompanied with a good plastic deformation. However, due to the less elongation and finer grain size in PWHT, a relatively smaller dimple features is expected for this type of samples in Figure 12(b). This type of fracture may prove that the crack was developed from the void in the interior of the structure and expanded under continued deformation until separation or fracture. Although, not all fractograph are shown. It is also worth to note that the welding orientation is an essential factor for influencing the type of fractography, for example, in WLRL fractured sample, a deep dimple fracture and multiple internal cracks can be observed.

4 Conclusions

This paper has presented the complete results of the influence of PWHT and welding orientation on the AL6061-T6 strength and microstructure characteristics. It is observed that both longitudinal and transversal welding orientation have only a slight difference on their mechanical performance, except after being heat-treated above 8 hours. The results have shown that on the specimens that undergo PWHT process, the increase in artificial aging period can significantly affect the grain growth after recrystallization, resulting in smaller grain size, especially for the WM specimens. Their microhardness is significantly increased and nearly uniform in the WM, HAZ, and BM compared to the as-welded specimen. It can be concluded that specimen from the T6-24 hours has the highest microhardness along with the smallest measured grain size. Subsequently, the tensile testing supports this result, showing the most superior of YS and UTS values is from the T6-24 hours for WLRL and WTRT specimens. The improvements in the strength and ductility were mainly contributed by the microstructural evolution as grain growth, dissolution, and precipitation hardening by Mg_2Si due to the artificial aging.

Acknowledgement: The authors would like to acknowledge the department of mechanical engineering of the Diponegoro University for providing any cost of this project.

References

[1] Ahmad R, Bakar MA. Effect of a post-weld heat treatment on the mechanical and microstructure properties of AL6061 joints welded by the gas metal arc welding cold metal transfer method. Mater Des. 2011;32:5120-6.

[2] Eltai E, Mahdi E, Alfantazi A. The effects of gas tungsten arc welding on the corrosion and mechanical properties of AL6061 T6. Int J Electrochem Sci. 2013;8:7004-15.

[3] Haryadi GD, Dewa RT, Ekaputra IMW. Fatigue crack growth and probability assessment for transverse TIG welded Aluminum alloy 6013-t4. J Theor App Mech-Pol. 2018;56(1):179-90.

[4] Ekaputra IMW, Haryadi GD, Mardikus S, Dewa RT. Probabilistic evaluation of fatigue crack growth rate for longitudinal tungsten inert gas welded Al 6013-T4 under various post weld heat treatment conditions. E3S Web Conf. 2019;130:01016.

[5] ASTM International. ASTM E384-16: 2016. Standard test method for microindentation hardness of materials. West Conshohocken, PA, USA: ASTM; 2016.

[6] ASTM International. ASTM B557-15: 2015. Standard test methods for tension testing wrought and cast aluminum- and magnesium-alloy products. West Conshohocken, USA: ASTM; 2015.

[7] ASTM International. ASTM E112-13: 2013. Standard test methods for determining average grain size. West Conshohocken, USA: ASTM; 2013.

[8] Nie F, Dong H, Chen S, Li P, Wang L, Zhao Z, et al. Microstructure and mechanical properties of pulse MIG welded 6061/A356 aluminum alloy dissimilar butt joints. J Mater Sci Technol. 2018;34:551-60.

[9] Liang Y, Hu S, Shena J, Zhang H, Wang P. Geometrical and microstructural characteristics of the TIG-CMT hybrid welding in 6061 aluminum alloy cladding. J Mater Process Technol. 2017;239:18-30.

[10] Maisonnette D, Suery M, Nelias D, Chaudet P, Epicier T. Effects of heat treatments on the microstructure and mechanical properties of A 6061 aluminium alloy. Mater Sci Eng A. 2011;528:2718-24.

[11] Boonchouytan W, Chatthong J, Rawangwong S, Burapa R. Effect of heat treatment T6 on the friction stir welded SSM 6061 aluminum alloys. Energy Procedia. 2014;56:172-80.

[12] Gussev MN, Sridharan N, Norfolk M, Terrani KA, Babu SS. Effect of post weld heat treatment on the 6061 aluminum alloy produced by ultrasonic additive manufacturing. Mater Sci Eng A. 2017;684:606-16.

[13] Lee WS, Tang ZC. Relationship between mechanical properties and microstructural response of 6061-T6 aluminum alloy impacted at elevated temperatures. Mater Des. 2014;58:116-24.

[14] Singh R, Chauhan S, Gope PC. Influence of notch radius and strain rate on the mechanical properties and fracture behavior of TIG-welded 6061 aluminum alloy. Arch Civ Mech Eng. 2016;16:513-23

[15] Feng AH, Chen DL, Ma ZY. Microstructure and low-cycle fatigue of a friction-stir-welded 6061 aluminum alloy. Metall Mater Trans A. 2010;41A:2626-41.

[16] Fadaeifard F, Matori KA, Aziz SA, Zolkarnain L, Zairie BA, Rahim MA. Effect of the welding speed on the macrostructure, microstructure and mechanical properties of Al6061-T6 friction stir butt welds. Metals-Basel. 2017;7:48.